THE PUBLISHING HOUSE
OF THE ROMANIAN ACADEMY

PROCEEDINGS OF THE ROMANIAN ACADEMY, Series A,
Volume 16, Number 2/2015, pp. 176–183

ANALYSIS OF THE SCISSION NEUTRONS BY A TIME-DEPENDENT APPROACH

M. RIZEA[1], N. CARJAN[1,2]

[1] "Horia Hulubei" National Institute for Physics and Nuclear Engineering, Department of Theoretical Physics
Str. Reactorului no. 30, P.O. BOX MG-6, Bucharest – Magurele, Romania
[2] Bordeaux University, Centre d'Etudes Nucleaires de Bordeaux-Gradignan, BP 120, 33175 Gradignan Cedex, France
Corresponding author: M.RIZEA, E-mail: rizea@theory.nipne.ro

In previous papers we studied the properties of the scission neutrons using two approaches: one stationary (the sudden approximation) and one time-dependent. The latter approach involves more complicated calculations but it is more realistic. In the frame of this approach we extend now our calculations to the time evolution of quantities such as: the spatial distribution of the emission points, the current density, the angular distribution with respect to the fission axis and the partition of v_{sc}^{em} (the number of emitted neutrons) among the light and the heavy fragments. The scission process is regarded as adiabatic transition from two fragments connected by a thin neck to two separated fragments. To follow this evolution we solve numerically the two-dimensional time-dependent Schrödinger equation with time-dependent potential. Calculations are performed for the nucleus ^{236}U at different mass divisions. The neutrons released during the scission are followed in time up to T_{max} = = 4×10^{-21} s. Their angular distribution is evaluated and compared with experimental data obtained in $^{235}U\,(n_{th}, f)$ reaction.

Key words: low-energy nuclear fission, scission neutrons, neutron multiplicity, probability and current densities, angular distribution with respect to the fission axis, bi-dimensional time-dependent Schrödinger equation, time-dependent potential.

1. INTRODUCTION

Nuclear fission of heavy elements was discovered by Otto Hahn and Fritz Strassmann [1] and explained theoretically by Lise Meitner and Otto Robert Frisch [2]. This discovery was important not only for fundamental nuclear physics but also for its applications, one of them being the energy supply through nuclear reactors. As main products of the nuclear reactions involved, the neutrons received, from the beginning, a special attention. Their study and evaluation are essential for the design of nuclear power plants, the safe operation of nuclear reactors, the handling of nuclear waste and the investigation of next-generation reactor systems and fuel cycles.

In the present study we are interested in the neutrons emitted during the scission process in low energy fission. The prompt neutrons accompanying fission are divided in two categories: scission neutrons and post-scission neutrons. The post-scission neutrons are supposed to be evaporated from fully accelerated fragments (*i.e.*, a long time after the division of the fissioning system into two fragments) and represent the majority. The scission neutrons are emitted due to the abrupt change of the nuclear shape (and potential) during the separation into two fragments. The different origin and properties of the scission neutrons and their influence on the whole fission process has become a subject of increasing interest. Attempts have been made to separate the yield of scission neutrons in low energy fission [3–5]. It was reported that the scission neutrons represent 10 – 20 % of the total number of fission neutrons. Since it is experimentally difficult to distinguish the scission neutrons, theoretical approaches are very useful. For this reason a dynamical model was developed recently. The simplest way to include dynamical effects is the sudden approximation [6, 7], based on the assumption that the transition from two fragments connected by a thin neck to two separated fragments happens infinitely fast (the scission time $\Delta T = 0$). In reality is fast but not sudden (ΔT is short but $\neq 0$). Therefore a time-dependent model is more adequate. It implies the numerical solution of the bi-dimensional time-dependent Schrödinger equation (TDSE2D) with time-dependent potential (TDP) – [8–10].

In the present paper we extend the application of this model [10] to the detailed study of the following properties of the scission neutrons as a function of time: probability and current densities of the unbound neutrons, their angular distribution with respect to the fission axis and the partition of the number of emitted neutrons among the light and the heavy fragments. Where possible, a comparison with experimental data is included. The final section is dedicated to the summary of the results.

2. TIME DEPENDENT SCHRÖDINGER EQUATION

Our numerical algorithm for the time propagation is explained in details in [8–10]. For completness the main points are reminded below.

The nuclear shape is assumed to be axially symmetric and we use cylindrical coordinates. The TDSE2D with TDP is:

$$\mathrm{i}\hbar\frac{\partial\Psi(\rho,z,\phi,t)}{\partial t}=H(\rho,z,\phi,t)\Psi(\rho,z,\phi,t). \tag{1}$$

The wavefunction has two components, corresponding to spin up and down:

$$\Psi(\rho,z,\phi,t)=f_1(\rho,z,t)\mathrm{e}^{\mathrm{i}\Lambda_1\phi}\,|\uparrow\rangle+f_2(\rho,z,t)\mathrm{e}^{i\Lambda_2\phi}\,|\downarrow\rangle, \tag{2}$$

where $\Lambda_1=\Omega-\frac{1}{2},\Lambda_2=\Omega+\frac{1}{2}$. Here Ω is the projection of the total angular momentum along the symmetry axis. Due to the axial symmetry, the dependence of ϕ is omitted. The Hamiltonian H has the form ([11]):

$$H\Psi=\begin{bmatrix}O_1-CS_c & -CS_a\\ -CS_b & O_2-CS_d\end{bmatrix}\begin{bmatrix}f_1\\ f_2\end{bmatrix},\quad O_{1,2}=-\frac{\hbar^2}{2\mu}\left(\Delta-\frac{\Lambda_{1,2}^2}{\rho^2}\right)+V(\rho,z,t),\ \Delta=\frac{1}{\rho}\frac{\partial}{\partial\rho}+\frac{\partial^2}{\partial\rho^2}+\frac{\partial^2}{\partial z^2}. \tag{3}$$

Here Δ is the Laplacean, V is the potential, C is a constant and the operators $S_a,\ldots,S_d$ represent the spin-orbit coupling. By the transformation $g_{1,2}=\rho^{1/2}f_{1,2}$ (Liouville), the first derivative from Δ is removed, resulting a simplified Hamiltonian $\hat{H}$ with the wavefunction $\hat{\Psi}$ having the components g_1,g_2 [8]. The TDSE2D becomes:

$$\mathrm{i}\hbar\frac{\partial\hat{\Psi}(\rho,z,t)}{\partial t}=\hat{H}(t)\hat{\Psi}(\rho,z,t). \tag{4}$$

We use a realistic mean field potential of Woods-Saxon type adapted to nuclear shapes described by generalized Cassini ovals [12] and we include a spin-orbit term. This shape parametrisation reproduces very accurately the optimal shapes at scission as function of mass asymmetry [13]. To numerically solve the TDSE2D we use the following scheme (of Crank- Nicolson type), which includes the derivative $\hat{H}'=\frac{\partial\hat{H}}{\partial t}$:

$$\left(1+\frac{\mathrm{i}\Delta t}{2\hbar}\hat{H}+\frac{\mathrm{i}\Delta t^2}{4\hbar}\hat{H}'\right)\hat{\Psi}(t+\Delta t)=\left(1-\frac{\mathrm{i}\Delta t}{2\hbar}\hat{H}-\frac{\mathrm{i}\Delta t^2}{4\hbar}\hat{H}'\right)\hat{\Psi}(t).$$

This scheme has important properties of stability and norm conservation. To apply the scheme, the infinite physical domain should be limited to a finite one, $[0,R]\times[-Z,Z]$, which is discretized by a grid with the mesh points: $\rho_j=j\Delta\rho$, $1\le j\le J$ ($\rho_J=R$), $z_k=k\Delta z$, $-K\le k\le K$ ($z_K=Z$). At each point the partial derivatives in $\hat{H}$ are approximated by finite difference formulas. For the derivatives with respect to z we use the standard 3-point formula, while for the derivatives in ρ, we deduced a special formula, which takes

into account the accomplished function transformation [8]. Let us denote $g_{jk}^{(n)}$ the approximation of g in the point (ρ_j, z_k) and at the time $t_n = n\Delta t$ (g is any of g_1 and g_2). The solution at t_{n+1}, represented by the values $g_{jk}^{(n+1)}$, is obtained in terms of the solution at time t_n, on the basis of the above Crank-Nicolson scheme, which turns into a linear system, after the discretization. It is solved by the conjugate gradient iterative method. As initial solution (at $t_0 = 0$) we take an eigenfunction of the stationary Schrödinger equation $\hat{H}\hat{\Psi} = E\hat{\Psi}$ The potential corresponds to the starting deformation. By using the same discretization of the Hamiltonian we arrive to an algebraic eigenvalue problem, which is solved by an appropriate method for large and sparse matrices (Arnoldi). During propagation in time, we apply transparent boundary conditions on the limits of the computational domain – e.g., [8]. This procedure avoids the reflexions on the numerical boundaries and allows relatively reduced grid sizes.

3. TWO-STEP TIME EVOLUTION

During the scission process different nuclear configurations appear. As mentioned, the nuclear shape is described in terms of Cassini ovaloids. This representation depends on a set of parameters; in our case we considered two: α (elongation) and α_1 (mass asymmetry). Let us denote by $\{\alpha^i\}$ the set corresponding to the just-before-scission configuration (when the neck starts to break) and by $\{\alpha^f\}$ the set corresponding to the immediately-after-scission configuration (when the neck stubs are completely absorbed by the fragments). The calculation of the time evolution is divided in two steps:

1. The transition $\alpha^i \to \alpha^f$. It happens in a relatively short time ($\Delta T \approx 10^{-22}$ sec). The nuclear potential changes rapidly and the neutrons that are present in the surface region are excited. For few of them, this excitation exceeds their binding and they are released.

2. The development after α^f. The neutrons left unbound move in the newly created potential of their interaction with the separated fragments. Their motion is considerably faster than that of the nascent fragments. Therefore, we will follow the evolution of the wave packet that describes the unbound neutrons assuming that the fragments remain in the configuration $\{\alpha^f\}$. Consequently, the potential in which the neutrons move is kept constant during this second phase. This separation of the neutrons from the fragments is calculated as a function of time up to a maximum value $t = T_{max}$.

The modeling of the above physical picture is accomplished through the numerical solution of the TDSE2D with (in phase 1) and without (in phase 2) TDP. Let $|\hat{\Psi}^i\rangle$, $|\hat{\Psi}^f\rangle$ be the eigenfunctions corresponding to $\{\alpha^i\}$ and $\{\alpha^f\}$ configurations, respectively. These functions along with the propagated wave functions $|\hat{\Psi}^i(t)\rangle$ that correspond at $t = 0$ to the eigenstates $|\hat{\Psi}^i\rangle$ will be used to calculate various physical quantities. Among them, the angular distribution with respect to the fission axis, which is supposed to be the best observable that could make the distinction between the scission neutrons and the evaporated ones.

4. PHYSICAL QUANTITIES

1. The probability that a neutron occupying the state $|\hat{\Psi}^i\rangle$ before scission populates a state $|\hat{\Psi}^f\rangle$ after a time interval T:

$$a_{if} = \langle\hat{\Psi}^i(T)\,|\,\hat{\Psi}^f\rangle = 2\pi\iint(g_1^i(T)g_1^f + g_2^i(T)g_2^f)\mathrm{d}\rho\mathrm{d}z.$$

2. The emitted part of the wave packet:

$$|\Psi_{em}^{i}\rangle = |\Psi^{i}(T)\rangle - \sum_{bound\ states} a_{if}\,|\Psi^{f}\rangle.$$

Note that above, the original functions (untransformed) are used.

3. The spatial distribution of the emission points:

$$S_{em}(\rho,z) = 2\times\sum_{bound} v_i^2\,|\Psi_{em}^{i}(\rho,z)|^2,$$

where the factor 2 is due to the spin degeneracy and v_i^2 are the occupation probabilities of each eigenstate, determined in the hypothesis of pairing correlations between neutrons. Alternatively, these probabilities may be deduced by assuming a nonzero temperature just before scission.

4. The current density, a vector defined as

$$\overline{J}_{em}^{i}(\overline{r},t) = \frac{\mathrm{i}}{\hbar}\frac{\hbar^2}{2\mu}(f\,\nabla f^{*} - f^{*}\,\nabla f).$$

We denoted by f the function $|\Psi_{em}^{i}\rangle$ and by $\overline{r}$ the spatial coordinate vector. In cylindrical coordinates we have:

$$\overline{J}_{em}^{i} = \frac{\mathrm{i}}{\hbar}\frac{\hbar^2}{2\mu}\left[\left(f\frac{\partial f^{*}}{\partial\rho} - f^{*}\frac{\partial f}{\partial\rho}\right)\overline{e}_{\rho} + \left(f\frac{\partial f^{*}}{\partial z} - f^{*}\frac{\partial f}{\partial z}\right)\overline{e}_{z}\right].$$

By writing $f = a + \mathrm{i}b$ we obtain:

$$\overline{J}_{em}^{i} = \frac{2}{\hbar}\frac{\hbar^2}{2\mu}\left[\left(ab_{\rho} - a_{\rho}b\right)\overline{e}_{\rho} + \left(ab_{z} - a_{z}b\right)\overline{e}_{z}\right] = J_{\rho}^{i}\overline{e}_{\rho} + J_{z}^{i}\overline{e}_{z}.$$

The components J_{ρ}^{i} and J_{z}^{i} (which are real numbers) of the vector $\overline{J}_{em}^{i}$ correspond to the state with the index i. The components for all states are obtained by summation:

$$J_{\rho}(\rho,z) = 2\times\sum_{i} v_i^2 J_{\rho}^{i}(\rho,z),\ J_{z}(\rho,z) = 2\times\sum_{i} v_i^2 J_{z}^{i}(\rho,z).$$

5. The number of neutrons that leave a sphere of radius R (around the fissioning nucleus) in a solid angle $\mathrm{d}\Omega$ and in a time interval $\mathrm{d}t$ is:

$$\mathrm{d}\nu_{\mathrm{sc}}^{\mathrm{em}} = \overline{J}_{em}(R,\theta,t)\,\overline{n}(R,\theta,t)\,R^2\,\mathrm{d}t\,\mathrm{d}\Omega.$$

Note that a transformation from cylindrical to spherical coordinates is needed. Actually, to calculate the angle θ and the normal $\overline{n}$ we use the closest values ρ, z of the cylindrical grid to the considered circumference as well as the corresponding values of J_{ρ} and J_{z}.

6. The angular distribution is given by the integral with respect to t of the above quantity. The upper limit should in principle be ∞. In practice we can reach only a finite value T_{max}.

7. The total number of emitted neutrons $\nu_{\mathrm{sc}}^{\mathrm{em}}$ at T_{max} is obtained by a further integration with respect to θ ($\mathrm{d}\Omega = \sin\theta\,\mathrm{d}\theta$). A factor of 4π also appears due to the integration over the angle ϕ and due to the spin degeneracy.

5. NUMERICAL RESULTS

We have investigated the nucleus ^{236}U at different mass asymmetries. We use a numerical domain defined by: $\rho\in[\Delta\rho,\,42]$, $z\in[-42,\,42]$, while $\Delta\rho = \Delta z = 0.125$ fm. The number of grid points is $\approx 226{,}000$. The time step is $\Delta t = 1/128\times10^{-22}$ s. The radius of the sphere is $R = 30$ fm and $R = 40$ fm,

while the depth of the nuclear potential is $V_0 = 40.22$ MeV. We considered for Ω the following values: 1/2, 3/2, 5/2, 7/2, 9/2, so that almost all initial states that are bound were taken into account. The deformations of the Cassini ovals before and after scission have the values: $\alpha^i = 0.985$ (corresponding to a neck radius $r_{min} = 1.6$ fm) and $\alpha^f = 1.001$ (corresponding to $d_{min} = 0.6$ fm, where d_{min} is the distance between the inner tips of the fragments along *z*-axis). The chosen value for r_{min} is slightly lower than the value predicted by the optimal scission shape [13]. Note that a zero neck scission shape has $\alpha = 1$. A second parameter α_1 is included in order to describe asymmetric fission ($A_L \neq A_H$, where A_L and A_H are the light and, respectively, the heavy fragment masses). The direction of the current density $\bar{J}_{em}(\rho,z,t)$ gives the direction of motion of the unbound neutrons in a point (ρ,z) at a time t. Its distribution provides a picture of the emission mechanism. Figure 1 shows this spatial distribution (arrows) at the end of the scission process ($\Delta T = 1\times10^{-22}$ s) and at two successive times T thereafter, together with the corresponding probability density i.e., the distribution of emission points (contour lines). To identify the neck position we added in each plot the equipotential lines corresponding to $V_0/2$ before and after scission. For illustration we have chosen a mass asymmetric case with the light fragment mass $A_L = 96$ (which is the most probable experimental mass asymmetry).

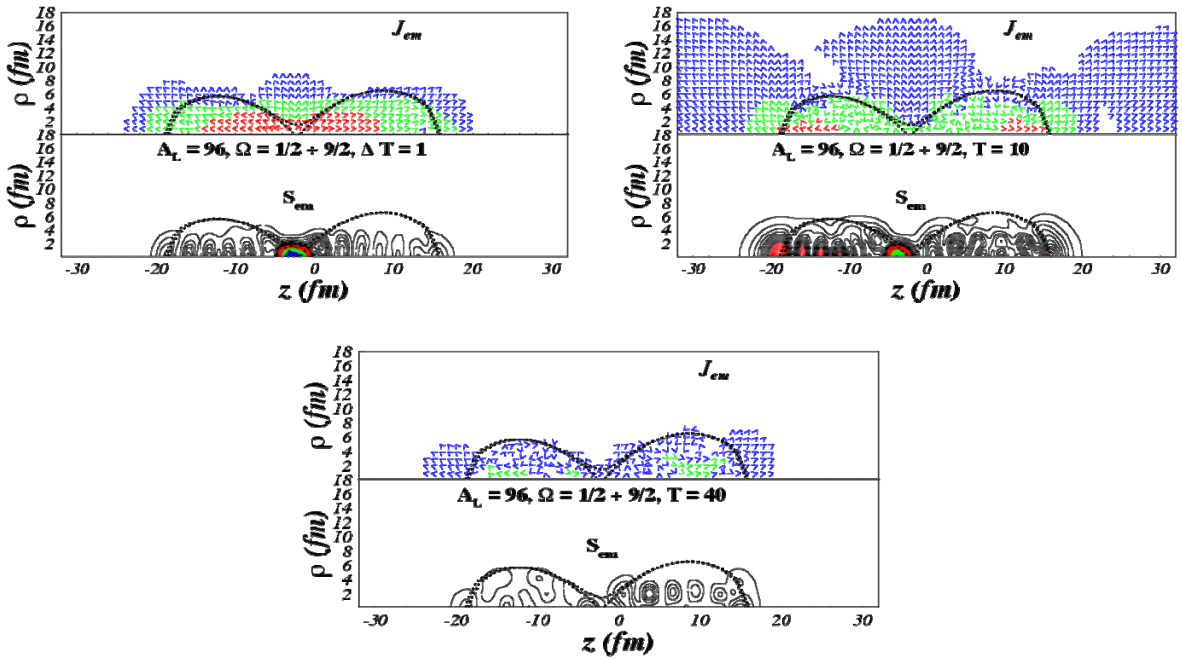

Fig. 1 – Distribution of average emission directions (arrows) of all the states associated to Ω from 1/2 to 9/2 for $A_L = 96$. The duration of the scission process is taken $\Delta T = 1\times10^{-22}$ s. Results at two subsequent time intervals $T = 10\times10^{-22}$ s and $T = 40\times10^{-22}$ s are also presented. The corresponding probability densities (contour lines) are shown in the lower part of each frame.

The intensity of the current $|\bar{J}_{em}|$ decreases strongly from inside to outside the fissioning system. Its highest three orders of magnitude are coded by colors (in decreasing order: red, green and blue). The represented current values are normalized to the maximum value at $\Delta T = 1\times10^{-22}$ s. One observes a progressively diminishing of the current intensity with the time. As expected, there is a correlation between $|\bar{J}_{em}|$ and S_{em}. The number of neutrons that leave the sphere of radius $R = 40$ fm (around the fissioning nucleus) – ν_{sc}^{em} – in terms of the mass asymmetry (defined by A_L) for different times T after scission is represented in Fig. 2. The results are obtained by summing over all Ω values. One can see that the variation

of the total number of neutrons with mass asymmetry is relatively weak (less than 10%). In Fig. 3 we represent ν_{sc}^{em} for each Ω set as a function of the primary fragment mass at T_{max}. In this way one can see the relative contribution of each set of wave functions and its distribution over the fragments masses. The separation between the neutrons emitted by the *L* and by the *H* fragments is done using the prescription of [7]. Likewise the number of unbound neutrons [6, 10], the number of neutrons crossing the sphere decreases with increasing Ω. The saw-tooth structure is present for all values, although has a slightly different form from one Ω value to another.

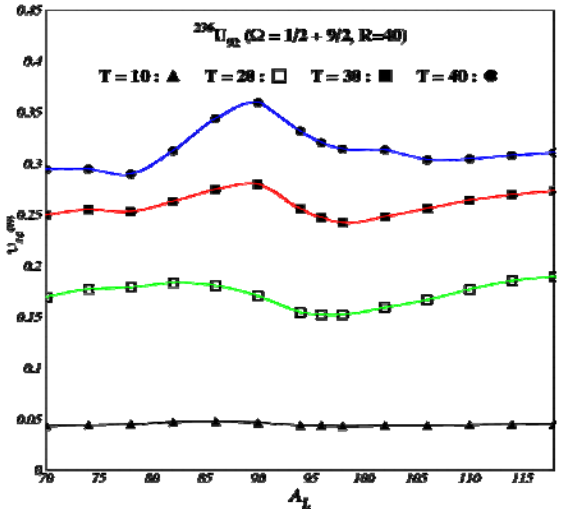

Fig. 2 – Number of scission neutrons that cross the sphere of radius *R* as a function of mass asymmetry up to different times *T* (in 10^{-22} s).

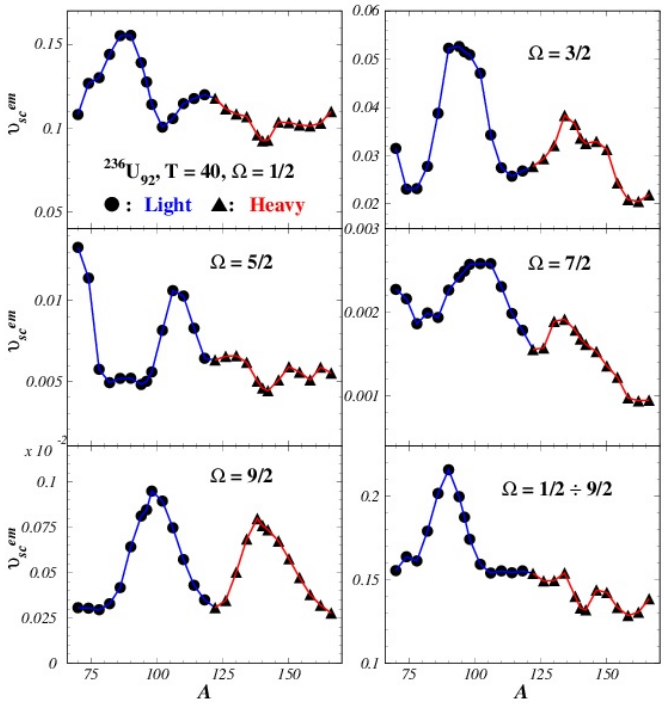

Fig. 3 – Contributions of each Ω set to scission neutron multiplicity in terms of the primary fragment mass at $T = 40$.

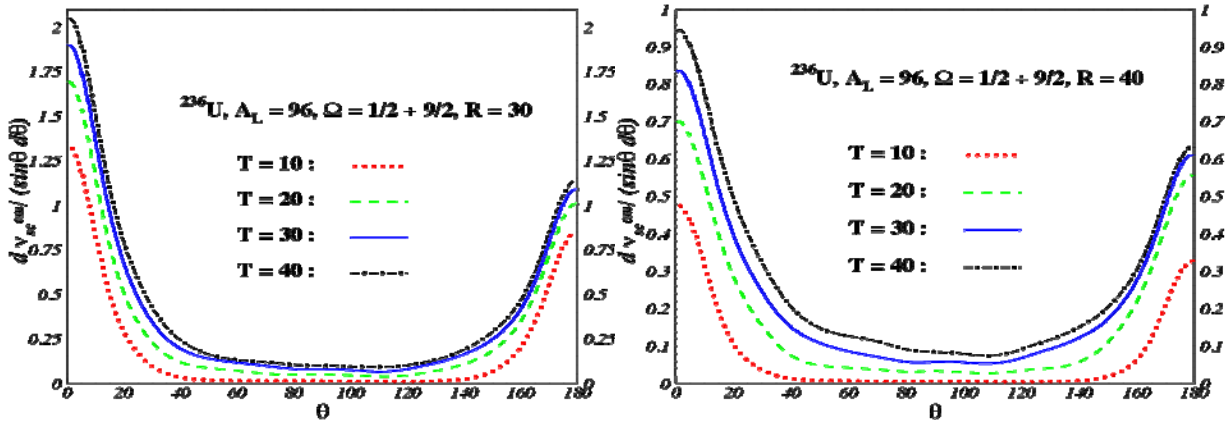

Fig. 4 – Angular distribution at different times *T* (in 10^{-22} s) after scission for the mass assymetry $A_L = 96$ and two sphere radii: 30 fm (left) and 40 fm (right).

In the following, angular distribution calculations are presented. Figure 4 contains results at different times T after scission for $A_L = 96$. To show the insensitivity of our calculations to the size of the numerical grid, two radii: $R = 30$ and $R = 40$ fm have been used. As it can be observed, the angular distribution has

two peaks: one in the direction of the light fragment and one in the direction of the heavy fragment. Due to the large CPU time required, we proceed our calculations until a limited time $T_{max} = 4\times10^{-21}$ s. This is however a relative long time at the scale of the process. At that time approximately 70% of the neutrons with positive energies left the sphere with $R = 30$ fm and 50% left the sphere with $R = 40$ fm. To compare with the experimental data one has to fold with the angular resolution function:

$$\frac{d\sigma}{d\theta}|_{\theta=\theta_0} = \int_{-\infty}^{\infty} \frac{d\sigma}{d\theta} r(\theta,\theta_0)d\theta,$$

where

$$r(\theta,\theta_0) = \frac{1}{\sqrt{2\pi}\varepsilon}\exp\left[-\frac{(\theta-\theta_0)^2}{2\varepsilon^2}\right]$$

and $\frac{d\sigma}{d\theta}$ is the angular distribution. The value of ε is obtained via the half width: $\varepsilon\sqrt{2\ln 2} = \Delta\theta_{1/2}$.

Since the experimental data represent an average over all possible mass fragments, we have obtained an averaged distribution from calculated distributions for a set of A_L values from 70 (a very asymmetric case) to 118 (the symmetric case). As weights we have used the mass yields from [14]. In Fig. 5 we compare the average distribution with the distribution corresponding to $A_L = 96$ (upper panel) and with the measured distribution [15] for the prompt neutrons (lower panel). As one can see, the average distribution and the distribution at $A_L = 96$ are very close. The calculated distributions have been folded with the angular resolution corresponding to $\Delta\theta_{1/2} = 16^{\circ}$. A remarkable resemblance with the experimental data is observed.

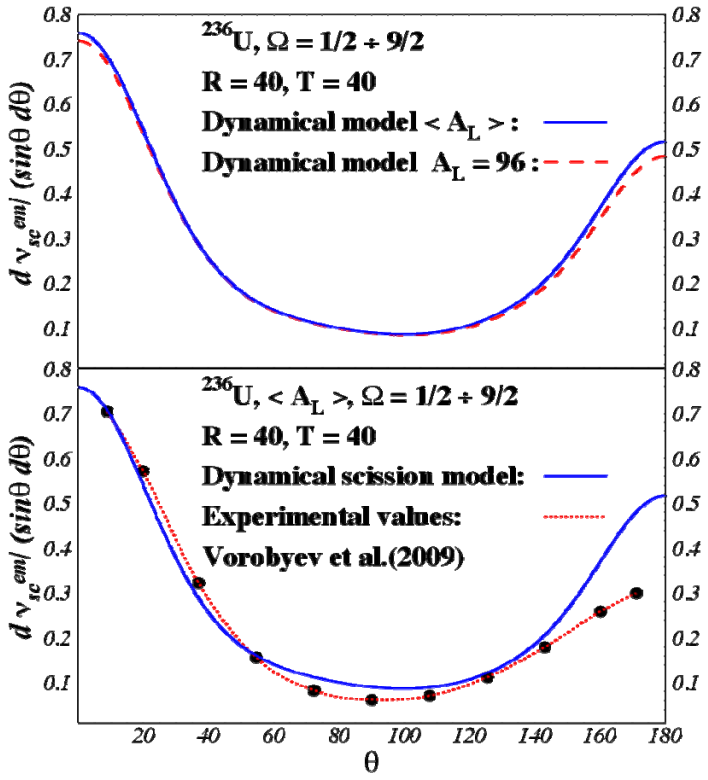

Fig. 5 – Comparison between the angular distribution with respect to the fission axis calculated for the scission neutrons and the measured distribution for the prompt fission neutrons (lower part). The average distribution is also compared with the distribution calculated for $A_L = 96$ (upper part). The notation $< A >$ means an averaging over a set of A_L.

6. SUMMARY

In the present paper a time-dependent approach to the scission process is used. The main computational problem is the solution of the TDSE2D with TDP. Detailed numerical results are obtained for the $^{235}U\,(n_{th}, f)$ reaction. In particular, snapshots of the neutron emission at scission are presented through spatial distributions of the probability and current densities at selected times *T*. These distributions clearly indicate an emission along the fission axis with preference for the light-fragment direction as observed experimentally in the case of prompt scission neutrons. The calculated variation of the scission neutron multiplicity as a function of the mass of the emitting fragment has a characteristic saw-tooth structure for each Ω value. Finally the angular distribution of the scission neutrons with respect to the fission axis was calculated, corrected for the experimental angular resolution and compared with measurements. A quantitative agreement was obtained.

Due to the complexity of the calculations we were forced to some limitations: a finite numerical spatial domain of reasonable size (compensated by Transparent Boundary Conditions implemented at the margins of the domain) and a not very large propagation time. However, even in these conditions, representative features of the scission neutrons were revelead and surprising similarities with the experimental data have been observed.

ACKNOWLEDGEMENTS

This work is partially supported by PN09370102 of the Romanian Ministry of National Education and by CNCS-UEFISCDI, project number PN-II-ID-PCE-2011-3-0068.

REFERENCES

1. O. HAHN, F. STRASSMAN, *Concerning the existence of alkaline earth metal resulting from neutron irradiation of uranium*, Naturwissenschaften, **27**, pp. 11–15, 1939.
2. L. MEITNER, O.R. FRISCH, *Disintegration of uranium by neutrons: a new type of nuclear reaction*, Nature, **143**, pp. 239–240, 1939.
3. H.R. BOWMAN, S.G. THOMPSON, J.C.D. MILTON, W.J. SWIATECKI, *Velocity and angular distributions of prompt neutrons from spontaneous fission of Cf-252*, Phys. Rev., **126**, pp. 2120–2136, 1962.
4. N.V. KORNILOV, A.B. KAGALENKO, S.V. POUPKO, P.A. ANDROSENKO, F.J. HAMBSCH, *New evidence of an intense scission neutron source in the Cf-252 spontaneous fission*, Nucl. Phys. A, **686**, pp. 187–203, 2001.
5. G.A. PETROV, *Current status of the search for scission neutrons in fission and estimation of their main chracteristics*, Nuclear Fission and Fission-Product Spectroscopy, AIP Conf. Proc., **798**, pp. 205–212, 2005.
6. N. CARJAN, M. RIZEA, *Scission neutrons and other scission properties as function of mass asymmetry in 235U(n-th,f)*, Phys. Rev. C, **82**, 014617, 2010.
7. N. CARJAN, F.-J. HAMBSCH, M. RIZEA, O. SEROT, *Partition between the fission fragments of the excitation energy and of the neutron multiplicity at scission in low-energy fission*, Phys. Rev. C, **85**, 044601, 2012.
8. M. RIZEA, N. CARJAN, *Computational study of scission neutrons in low-energy fission: stationary and time-dependent approaches*, Commun. Comput. Phys., **9**, pp. 917–936, 2011.
9. N. CARJAN, M. RIZEA, *Dynamic single particle excitations in low-energy fission*, Rom. J. Phys., **57**, pp. 92–105, 2012.
10. M. RIZEA, N. CARJAN, *Dynamical scission model*, Nucl. Phys. A, **909**, pp. 50–68, 2013.
11. J. DAMGAARD, H.C. PAULI, V.V. PASHKEVICH, V.M. STRUTINSKY, *A method for solving the independent-particle Schrödinger equation with a deformed average field*, Nucl. Phys. A, **135**, pp. 432–444, 1969.
12. V.V. PASHKEVICH, *On the asymmetric deformation of fissioning nuclei*, Nucl. Phys. A, **169**, pp. 275–293, 1971.
13. F. IVANYUK, *The shapes of conditional equilibrium in the liquid-drop model*, Int. J. Mod. Phys. E, **18**, pp. 879–884, 2009.
14. J.Ch. SUBLET, A.J. KONING, R. A. FORREST, J. KOPECKY, The JEFF□3.0/*A Neutron Activation File-New Features,Validation, and Usage*, AIP Conf. Proc., **769**, pp. 203–206, 2005.
15. A.S. VOROBYEV, O.A. SHCHERBAKOV, YU.S. PLEVA, A.M. GAGARSKI, G.V. VAL'SKI, G.A. PETROV, V.I. PETROVA, T.A. ZAVARUKHINA, *Measurements of angular and energy distributions of prompt neutrons from thermal neutron-induced fission*, Nucl. Inst. Meth. Phys. Res. A, **598**, pp. 795–801, 2009.

Received December 15, 2014